Lithium intercalation in TiO_2 modifications

Gerhard Nuspl,[a] Kazunari Yoshizawa[b] and Tokio Yamabe*[a,b]

[a]*Institute for Fundamental Chemistry, 34–4 Takano-Nishihiraki-cho, Sakyo-ku, Kyoto 606, Japan*
[b]*Department of Molecular Engineering, Kyoto University, Sakyo-ku, Kyoto 606–01, Japan*

Lithium intercalation in anatase and TiO_2 (B), a synthetic TiO_2 polymorph, is analyzed from approximate crystal orbital calculations. As a consequence of lithium incorporation, weak Ti—Ti bonding interactions are formed in both compounds. These bonding interactions lead to one-dimensional zigzag chains in the frameworks of anatase and TiO_2 (B). Extended Hückel calculations show that a small distortion of the anatase network is required to achieve Ti—Ti bonds, whereas such a distortion is not necessary in TiO_2 (B).

For many years a large number of natural and synthetic transition metal compounds which reversibly incorporate a remarkable amount of lithium are considered as possible electrode materials in solid-state lithium batteries.[1] These are, for example, layered compounds of transition-metal chalcogenides such as TiS_2, $TiSe_2$ or $TiTe_2$.[2–13] Another class is composed of many transition-metal oxides which are based on frameworks with tunnel systems; these systems have been investigated intensively as possible 'hosts' for lithium intercalation.[1,3–6,14–19] One material which promises excellent properties for technological use as an electrode material in solid-state lithium batteries is TiO_2.[20–22] Recently a lithium ion battery with nanostructured TiO_2 (anatase) as the anode and $LiCoO_2$ or $LiNi_{0.5}Co_{0.5}O_2$ as the cathode is under development.[21,22] Electrochemical studies have shown that the various modifications of TiO_2 incorporate lithium in different ratios.[23–37] Whereas brookite[38,39] and rutile[40–43] insert only small amounts of lithium,[23–29] anatase[40] and the synthetic polymorph TiO_2 (B)[36] react extensively with stoichiometries up to 0.8–1 Li per Ti.[28–37] TiO_2 (B) is prepared by hydrolysis of $K_2Ti_4O_9$ and subsequent heating to 500 °C.[36] The framework of TiO_2 (B) is metastable and transforms slowly into anatase at higher temperatures.

Let us first look at the natural mineral anatase [Fig. 1]. The three-dimensional network of anatase consists of strongly distorted edge sharing TiO_6 octahedra.[40] Since the space group of anatase is $I4_1/amd$, the framework is equivalent in [100] and [010] directions. The anatase structure can be considered as a stacking of one-dimensional zigzag chains A and B consisting of distorted edge-sharing octahedra. This stacking, equivalent in [100] and [010] directions, leads to empty zigzag channels in the anatase framework. The spheres in Fig. 1 mark possible positions of lithium insertion in anatase. Filling all sites leads to a stoichiometry of $LiTiO_2$ (anatase),[28–37] but this is unlikely to be a real situation. Lithium occupies highly distorted octahedral interstices in the anatase network which is better described as a five-fold coordination of lithium with oxygen.

Remarkable lithium intercalation was also observed in the polymorph TiO_2 (B).[29,36,37] The framework of the idealized TiO_2 (B) structure [Fig. 2] is a shear derivative of the ReO_3 type structure. In Fig. 2 the octahedra of A represent a first 'sheet' of corner sharing octahedra (ReO_3 blocks) and edge-sharing octahedra. The next 'sheet' B is equivalent to 'sheet' A, but moved by half of the unit cell length, *a*, in the [100] direction. The 'sheets' A and B are connected by edge sharing octahedra resulting in a three-dimensional framework. As a result of this connection, TiO_2 (B) shows a system of one-dimensional infinite channels in 'sheet' A and B which are following the [001] direction. In these channels lithium can be inserted and is expected to be very mobile. The maximal insertion rate of lithium in TiO_2 (B) is about 0.85 Li per Ti at 25 °C.[29,36,37]

Recently lithium intercalation in rutile and anatase has been investigated from Hartree–Fock calculations with the periodic large unit cell (LUC) method.[44] Equilibrium geometries and effective atomic charges were calculated for the lithium intercalation in rutile and anatase. A higher probability of lithium intercalation was predicted for anatase than for rutile. The

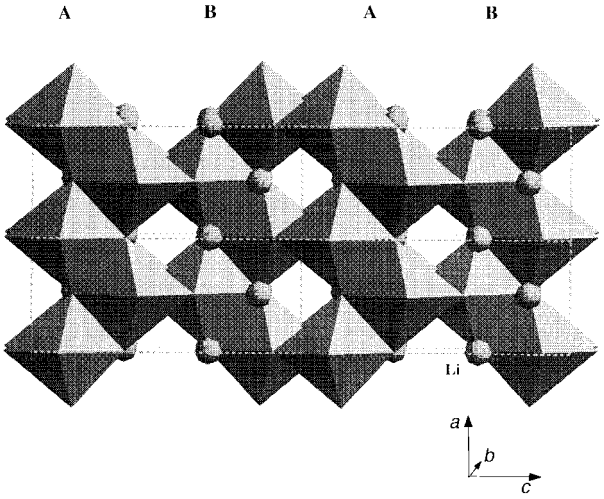

Fig. 1 Structure of the natural mineral anatase

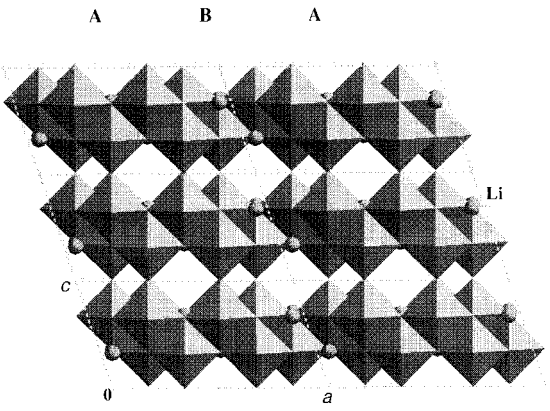

Fig. 2 Idealized TiO_2 (B) structure

purpose of this paper is to perform a detailed analysis of the lithium intercalation in anatase. The main emphasis of this work is a development of the bonding properties in the intercalated systems by using the crystal orbital overlap population (COOP) formalism[45] of the extended Hückel method.[46] Additionally we expanded our investigation to the lithium intercalation in TiO_2 (B). In the following section, we first consider the electronic and bonding properties of the lithium intercalation in anatase.

Lithium intercalation in anatase

The maximal lithium content in anatase is in the range of 0.5–1 Li per Ti, depending on experimental technique and temperature.[29–35] Our investigations are based on the observed crystallographic data for $Li_{0.5}TiO_2$ (anatase) obtained by neutron diffraction powder profile analysis.[47] Fig. 3 shows the framework of $Li_{0.5}TiO_2$ (anatase) which is abbreviated as $Li_{0.5}TiO_2$ (A). The symmetry is lowered from $I4_1/amd$ in anatase to *Imma* in $Li_{0.5}TiO_2$ (A). In $Li_{0.5}TiO_2$ (A) ($Z=4$) lithium is statistically distributed over one four-fold site 4(e) in *Imma*, because only half of the crystallographic sites are occupied. In Fig. 3 all possible sites of lithium intercalation are shown leading to a final stoichiometry of $LiTiO_2$ (A). As a result of lithium intercalation, the deviation of the TiO_6 octahedra from regularity decreases in $Li_{0.5}TiO_2$ (A). However, altogether the anatase framework is not very much distorted after lithium insertion. From crystal data, there are two sets of Ti—Ti distances, 2.887 and 3.128 Å,[47] which indicate possible Ti—Ti interactions along the [010] direction.

Let us first look at the density of states (DOS) of anatase and of $Li_{0.5}TiO_2$ (A) shown in Fig. 4. The hatched areas in Fig. 4(*a*) and (*b*) indicate the contribution of titanium. The dotted horizontal line marks the Fermi level. There is no drastic difference between the DOS of anatase and of $Li_{0.5}TiO_2$ (A). Thus, in a first qualitative view, lithium transfers its valence electron to the host lattice and enters the one-dimensional channels as an Li^+ ion denoted by $Li_x^{x+}(TiO_2)^{x-}$. The average net charge of lithium (+1.07) determined by a Mulliken population analysis supports a complete ionic formulation. Therefore, the lithium intercalation can be viewed as a filling of titanium d levels by neglecting the influence of lithium levels. The partly filled titanium levels are the t_{2g} set in an ideal octahedral coordination. Such a behaviour is expected for compounds which are able to incorporate lithium easily and reversibly.

Since the structural change should be small as a function of composition for solid-state cathode materials,[14] there should be no drastic change in the electronic nature of the framework. However, there are important differences between the electronic properties of the two compounds. Therefore let us next look

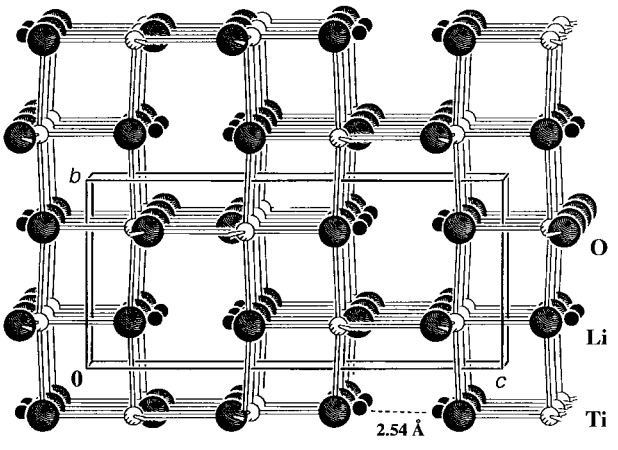

Fig. 3 Framework structure of $Li_{0.5}TiO_2$ (anatase)

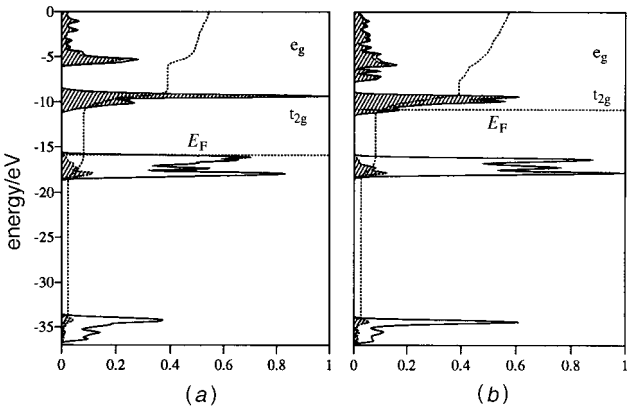

Fig. 4 Density of states (DOS) of (*a*) anatase and (*b*) $Li_{0.5}TiO_2$ (A). Shaded regions correspond to the contribution of titanium and the dotted lines running upwards indicate the integrations of the projected titanium levels. The dotted horizontal lines mark the Fermi level.

at the projected DOS of the d_{xy}, d_{yz} and d_{xz} orbitals in Fig. 5. In the following the labeling of the d levels is in agreement with the unit cell directions *x*, *y* and *z*.

The t_{2g} set of the titanium d orbitals of an ideal octahedral symmetry is further split in anatase and in $Li_{0.5}TiO_2$ (A) (Fig. 6), because the local TiO_6 geometry is lowered from O_h in an idealized framework to D_{2d} and C_{2v}, respectively. This splitting of the t_{2g} set which can be easily derived by using arguments of ligand-field theory is still visible in the projected DOS of the three-dimensional framework of $Li_{0.5}TiO_2$ (A) [Fig. 5(*a*)–(*c*)].

In $Li_{0.5}TiO_2$ (A), the tetragonal symmetry of anatase changes to orthorhombic symmetry by splitting the equal O—Ti—O angles of 155.3° in anatase to 158.9° and 175.0° in $Li_{0.5}TiO_2$ (A). Since the O—Ti—O angle in [010] direction changes by 16.1°, the distortion from regularity of the TiO_6 'octahedron' is smaller for $Li_{0.5}TiO_2$ (A) than for anatase. Therefore, going from anatase to $Li_{0.5}TiO_2$ (A), the d_{yz} bands are lowered in energy and lying close to the d_{xy} levels. We will see later that a different splitting of the d levels in anatase and $Li_{0.5}TiO_2$ (A) is responsible for a change in the bonding properties of the titanium atoms.

What is the reason for the distortion of the host Ti—O lattice in $Li_{0.5}TiO_2$ (A)? In order to answer this question, crystal orbital overlap population (COOP) curves were calculated for different Ti—O and Ti—Ti distances. To allow a fair comparison, all Ti—O bonds were fixed at their average length of 1.95 Å in anatase and at 2.0 Å in $Li_{0.5}TiO_2$ (A).

The bond angles in the distorted octahedra remain at their experimentally determined values shown in anatase and $Li_{0.5}TiO_2$ (A). This assumption leads to a Ti—Ti distance of 3.0 Å (exptl. 3.04 Å) in anatase and two different Ti—Ti distances of 2.91 and 3.08 Å in $Li_{0.5}TiO_2$ (A) (exptl. 2.89 and 3.13 Å). In Fig. 7 the COOP curves are drawn for the Ti—Ti bonds in anatase and $Li_{0.5}TiO_2$ (A). For simplicity, the different bond types are labeled [A] and [B] in anatase and $Li_{0.5}TiO_2$ (A) (Fig. 8). Positive and negative regions indicate bonding and antibonding interactions, respectively.

In anatase the d_{xy} levels are first occupied with electrons after lithium insertion. For these d_{xy} levels no bonding character is expected because the nearest Ti neighbour for a $\pi(d_{xy}^{Ti}–d_{xy}^{Ti})$ interaction is 3.784 Å apart. Increasing the number of electrons above 0.5 e per Ti, the d_{xz} and d_{yz} levels are also more and more filled. The $\sigma(d_{yz}^{Ti}–d_{yz}^{Ti})$ and $\sigma(d_{xy}^{Ti}–d_{xy}^{Ti})$ interactions between nearest neighbouring Ti atoms (3.04 Å) are antibonding, due to the distortion of the ideal octahedron geometry. In the energy region between −10 and −8.5 eV, these antibonding Ti—Ti interactions lead to a large negative peak in the COOP curve [Fig. 7(*a*)]. Thus, our

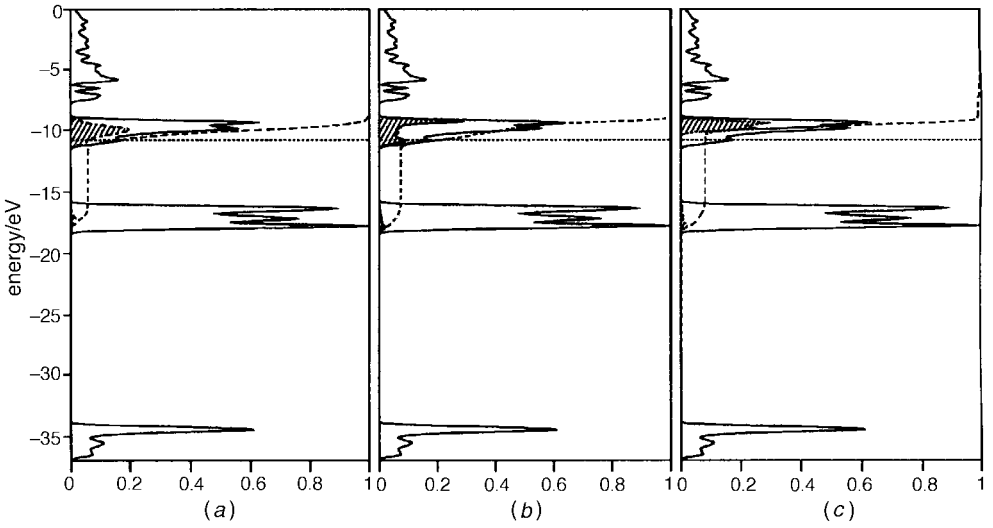

Fig. 5 Projected DOS of titanium: (*a*) 3 d_{xy} levels, (*b*) 3 d_{yz} levels and (*c*) 3 d_{xz} levels in $Li_{0.5}TiO_2$ (A). Solid lines in the DOS plots give the total DOS, while shaded regions correspond to the projections. The dashed lines running upwards are the integrations of the projected scale.

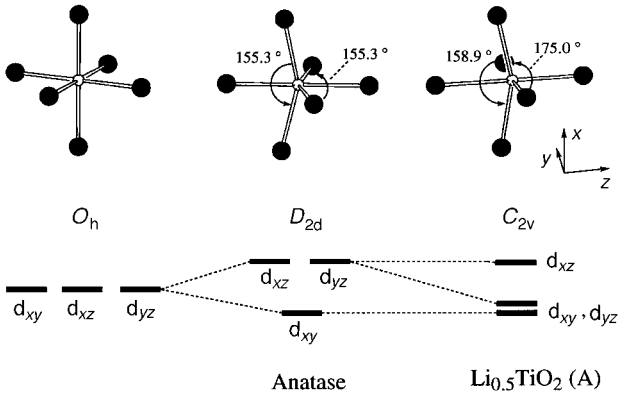

Fig. 6 Splitting of titanium d orbitals in going from ideal O_h symmetry to anatase (D_{2d}) to $Li_{0.5}TiO_2$ (A) (C_{2v})

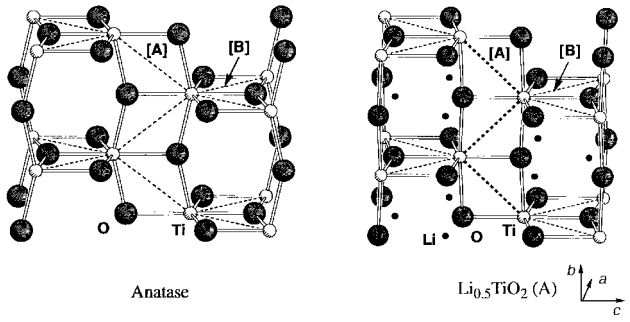

Fig. 8 Bond types [A] and [B] in idealized anatase and $Li_{0.5}TiO_2$ (A)

first conclusion is that if anatase incorporates lithium without any distortion of its framework, titanium levels with strongly antibonding character will be filled. As a result, a destabilization of the framework should be expected by intercalation of lithium.

However, the anatase framework can balance this unfavorable electronic situation, due to lithium intercalation, by slightly distorting the network in the [010] direction. Since one O—Ti—O angle changes from 155.3° in anatase to 175° in $Li_{0.5}TiO_2$ (A), the d_{yz} levels are lowered in energy. As a consequence of the d_{yz} levels lying below the Fermi level in $Li_{0.5}TiO_2$ (A), strong zigzag $\sigma(d_{yz}^{Ti}–d_{yz}^{Ti})$ bonding interactions are 'switched on' in [A]. In $Li_{0.5}TiO_2$ (A) (Fig. 8) the bonding character of [A] is emphasized by a doubled dashed line. By comparing the COOP curves of Fig. 7(*a*) and (*b*), it is evident

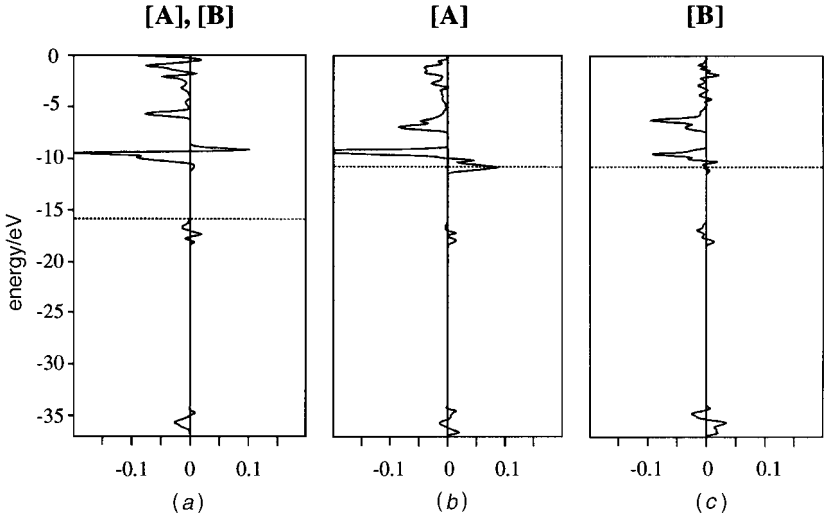

Fig. 7 Crystal orbital overlap population (COOP) curves for (*a*) Ti—Ti bond [A] and [B] in an idealized anatase structure [d(Ti—O) = 1.95 Å], (*b*) Ti—Ti bond [A] in an idealized $Li_{0.5}TiO_2$ (A) structure [d(Ti—O) = 2.0 Å] and (*c*) Ti—Ti bond [B] in an idealized $Li_{0.5}TiO_2$ (A) structure

that they are completely different for [A] in anatase and $Li_{0.5}TiO_2$ (A). In the energy region of −11.3 to −10 eV, there is a change from antibonding character in anatase to bonding character in $Li_{0.5}TiO_2$ (A). A detailed analysis shows that the bonding character of $Li_{0.5}TiO_2$ (A) originates from bonding d_{yz} levels. In the undistorted anatase [Fig. 7(*a*)] these bonding d_{yz} levels are located at higher energy about −8.5 to −9 eV. Experimentally, the formation of bonding Ti—Ti zigzag chains is suggested by the non-metallic resistivity of lithium-doped anatase which would not be expected if the electrons are delocalized over the whole Ti—O framework.[47]

In contrast to the energetic shift of the bonding d_{yz} levels, the nature of the d_{xy} and d_{xz} levels in [A] is not much affected by the distortion of the framework. Thus, in $Li_{0.5}TiO_2$ (A) the $\pi(d_{xy}^{Ti}–d_{xy}^{Ti})$ interactions are still non-bonding and the $\sigma(d_{xz}^{Ti}–d_{xz}^{Ti})$ interactions located above −10 eV are still antibonding.

Contrary to bond [A] the general features of the COOP curve of the longer Ti—Ti bond [B] of 3.13 Å are very similar to those of anatase [Fig. 7(*a*) and (*c*)]. This is not surprising, because the distortion of the original anatase framework is very small in the [100] direction (the O—Ti—O angle changes from 155.3 to 158.9°). Since the bond [B] is longer in $Li_{0.5}TiO_2$ (A) than the corresponding one in anatase, the interactions are smaller in $Li_{0.5}TiO_2$ (A). As a consequence, the formation of bonding Ti—Ti zigzag chains is expected only in the [010] direction.

Let us next look at the behaviour of the average overlap population (AOP) for the Ti—Ti bond [A] with varying lithium content. In Table 1 the AOP of the complete $Li_{0.5}TiO_2$ (A) structure is compared to an electron filling of an $Li_{0.5}TiO_2$ (A) like $(TiO_2)^{x-}$ framework and to a hypothetical electron filling of the original anatase network. Again, all Ti—O distances are fixed at the average observed value of 2.0 Å in Li_xTiO_2 (A) and $(TiO_2)^{x-}$, and at 1.95 Å in anatase.

The trends of the AOP for Li_xTiO_2 (A) and anatase confirm our previous discussion and follow the features of the COOP curves shown in Fig. 7(*a*)–(*c*). Without lithium insertion ($x=0$) weak antibonding interactions are expected for [A] in Li_xTiO_2 (A), but with increasing lithium content the AOP indicates more and more bonding character for the Ti—Ti bond [A]. In contrast to this change, the AOP for the original anatase framework remains antibonding for [A] after lithium intercalation. However, since lithium levels are slightly mixing into the bonding $\sigma(s^{Ti}–s^{Ti})$ bands, the latter are stabilized in energy. This effect increases by inserting more and more lithium and enlarges the AOP to higher positive values. In order to omit this additional effect, we also show the AOP of an $Li_{0.5}TiO_2$ (A) like $(TiO_2)^{x-}$ framework in Table 1. Since a similar increase in bonding character is observed for an electron filling in a $(TiO_2)^{x-}$ network, the formation of Ti—Ti bonds is likely to be a driving force for the small distortion of the original anatase network.

In the last section we suggested a stabilization of the anatase framework by a small distortion of the original framework and by the formation of bonding Ti—Ti interactions. However, the stability of the network is also determined by the magnitude of the Ti—O interactions. Thus, let us next look at the COOP curves for the four different Ti—O bonds shown in Fig. 9 ($d=2.0$ Å). The general features of these four Ti—O bonds are very similar, and in the same way as Ti—Ti $\sigma(d_{yz}–d_{yz})$ bonding is created by lithium insertion, antibonding $\pi^*(d^{Ti}–p^O)$ interactions are getting more and more dominant with increasing lithium content. However, up to a lithium content of 1 Li per Ti, only $\pi^*(d^{Ti}–p^O)$ levels with small antibonding character are occupied. From a close inspection of Fig. 9 it is obvious that strongly antibonding levels will be occupied if we hypothetically increase the number of additional electrons above 1e per Ti.

Thus, assuming a qualitative picture of a negatively charged $(TiO_2)^-$ host lattice, where lithium transfers its electron to the framework, we expect only a small decrease in the Ti—O bond strength with increasing lithium insertion in the region of $0<x<1$. Moreover, performing an extended Hückel calculation which includes lithium atoms, also another effect becomes important for the Ti—O bonds (Fig. 10). By small mixing of Ti s and O s levels with Li s levels, the $\sigma(s^{Ti}–s^O)$ bond character is influenced by lithium insertion. The magnitude of this mixing is strongly dependent on the sites of the inserted lithium with respect to the Ti—O bond and on the varying lithium content. By averaging over all four Ti—O bonds which are equal in distance (2.0 Å) in our idealized structure, the AOP for Ti—O in Li_xTiO_2 is listed in Table 2. The occupation of antibonding $\pi^*(d^{Ti}–p^O)$ levels becomes more and more dominant if the amount of lithium is increased beyond 0.5 Li per Ti. Even so, for $0<x<1$, no significant change of the averaged Ti—O bond strength is expected from our results. A strong destabilization of the Ti—O bonds is only predicted for a hypothetical filling of Ti d levels beyond

Table 1 Average overlap population for the Ti—Ti bond [A] as a function of lithium content x in idealized structures of Li_xTiO_2 (A), $(TiO_2)^{x-}$, and anatase. All Ti—O bonds are fixed at 2.0 Å in Li_xTiO_2 (A) and $(TiO_2)^{x-}$, and at 1.95 Å in anatase

x:	0	0.25	0.5	0.75	1
Li_xTiO_2 (A)	−0.014	0.018	0.048	0.066	0.082
$(TiO_2)^{x-}$	−0.014	0.001	0.016	0.028	0.036
anatase[a]	−0.020	−0.017	−0.016	−0.020	−0.024

[a]Hypothetical electron filling of the original anatase framework [no distortion as in Li_xTiO_2 (A) and $(TiO_2)^{x-}$].

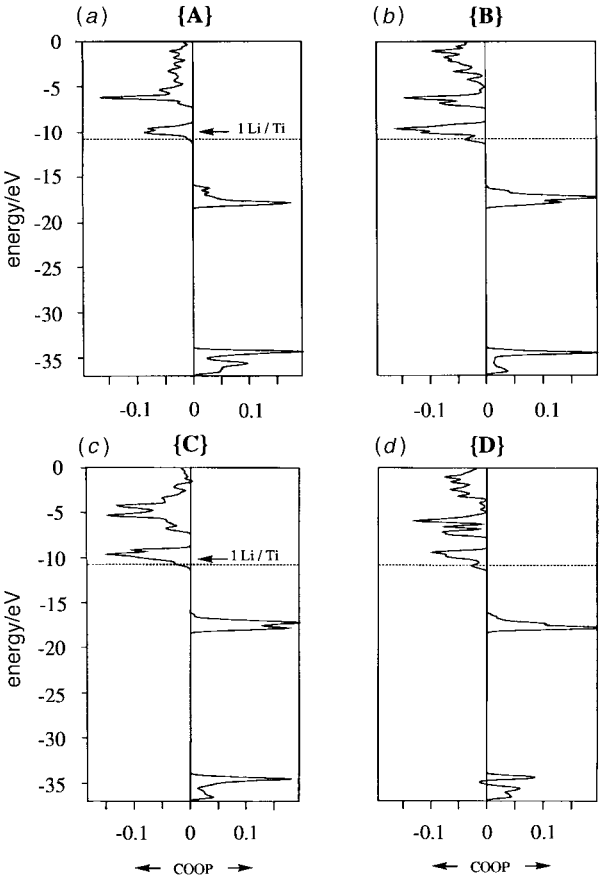

Fig. 9 COOP curves for (*a*) Ti—O bond {A}, (*b*) Ti—O bond {B}, (*c*) Ti—O bond {C} and (*d*) Ti—O bond {D} in an idealized $Li_{0.5}TiO_2$ (A) structure ($d=2.0$ Å). The arrow marks the Fermi level for an insertion of 1 Li per Ti.

Table 2 Average overlap population over all Ti—O bonds as a function of lithium content in an idealized Li_xTiO_2 (A) structure ($d = 2.0$ Å)

	TiO_2 (A)	$Li_{0.25}TiO_2$ (A)	$Li_{0.5}TiO_2$ (A)	$Li_{0.75}TiO_2$ (A)	$LiTiO_2$ (A)
AOP	0.308	0.317	0.320	0.318	0.315

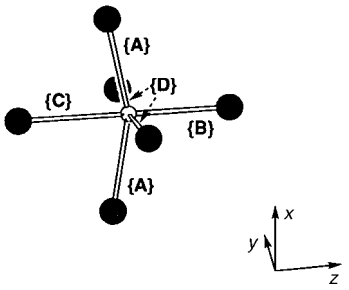

Fig. 10 Bonds {A}–{D} in idealized $Li_{0.5}TiO_2$ (A)

1.0 electrons per Ti. As a consequence of the AOP, the stability of the anatase framework with respect to the Ti—O bonds is hardly affected either by lithium incorporation or by the distortion of the framework. The formation of Ti—Ti bonds determines the direction of distortion, as we mentioned above.

Let us next consider the electronic nature of the inserted lithium ions. In $Li_{0.5}TiO_2$ the intrachain Li—Li distance within the [100] channels is 2.54 Å determined with neutron diffraction powder techniques.[47] The interchain Li—Li distance is 3.50 Å. The computational results indicate that there is no Li—Li interaction in $Li_{0.5}TiO_2$ (A). The AOP of −0.02 for the shortest Li—Li distance of 2.54 Å is about 10% of the AOP of a hypothetical Li—Li zigzag chain with the same distance of 2.54 Å. We expect that these weak interactions will be overcome by Coulombic nuclear–nuclear repulsion. As suggested by Cava *et al.*,[47] the repulsive Coulombic forces are mainly responsible for the limitation of the possible lithium content to 0.7 Li per Ti. On the one hand, the number of repulsive interactions increases rapidly above 0.5 Li per Ti as a result of more and more Li—Li neighbours at 2.54 Å. Moreover, our results suggest a further distortion of the anatase network in the direction towards the ideal octahedral environment due to strengthening of Ti—Ti bonds with increasing electron number. Simultaneously, as a geometric consequence of further distortion, the Li—Li distance of 2.54 Å has to become smaller.

Previous experimental work on lithiated rutiles suggested a comparable formation of metal–metal interactions.[27] Especially in RuO_2 and OsO_2 the c/a ratio of the tetragonal unit cell of the rutile structure becomes smaller after lithium insertion which indicates significant metal–metal bonding. In contrast to the rutile compounds where the incorporation of lithium is accompanied by a drastic increase of the unit-cell volume between 11 and 18%, the volume increase in anatase is only 3% after lithium intercalation. The small structural change in the anatase structure is very important for a good solid state cathode material (resulting in a reversible reaction). Our computational results show that the anatase framework is very versatile and can easily balance a change in electron count by a small and reversible geometrical adjustment. No Ti—O bond cleavage is necessary; the distortion is only stabilized by the formation of weak Ti—Ti bonds.

Lithium intercalation in TiO_2 (B)

TiO_2 (B) was first described by Marchand *et al.* in 1980.[36] They also determined the highest content of lithium to be $Li_{0.85}TiO_2$ (B). Later investigations on the lithium incorporation in TiO_2 (B) performed by Zachau-Christiansen *et al.* in 1988[29] are in full agreement with the earlier results.[36,37]

Since only unit-cell parameters, but no fractional coordinates are published for TiO_2 (B) and the Li_xTiO_2 (B) compounds, we assumed an ideal TiO_2 (B) network with an ideal octahedron geometry and equal Ti—O bond distances of 2.03 Å. $Li_{0.5}TiO_2$ (B)[29] is isotypic to $Li_2FeV_3O_8$[48] which was characterized by neutron diffraction powder techniques. In $Li_2FeV_3O_8$ where Fe and V are statistically distributed over a TiO_2 (B)-like framework, the octahedra are slightly deformed from ideal geometry resulting in a minimal distortion of the host lattice. In this compound the incorporated lithium ions are coordinated to oxygen in an LiO_5 polyhedron which is best described as a slightly distorted square pyramid. Similar to the intercalation in anatase, lithium prefers five-fold coordination in TiO_2 (B) [Fig. 11(*a*)]. NMR investigations indicate that equivalent crystallographic sites are occupied in $Li_{0.5}TiO_2$ (B).[29,36,37] Fig. 11(*b*) shows these pentacoordinated positions in the TiO_2 (B) host lattice. The dark circles representing lithium mark the sites which are occupied in $Li_{0.5}TiO_2$ (B) by analogy with those of $Li_2FeV_3O_8$ (B). In TiO_2 (B) there are further vacant sites for intercalation with fivefold coordination. These sites are visible in Fig. 2 by a complete filling of the zigzag channels. Occupying all available sites leads to a stoichiometry of Li_1TiO_2.

Let us first look at the DOS curve of TiO_2 (B) shown for the idealized structure in Fig. 12. The solid line indicates the total DOS, and the hatched areas the contribution from titanium. The total DOS of $Li_{0.5}TiO_2$ (B) (not shown here) is very similar to that of TiO_2 (B). Again, the incorporation of lithium is more or less just a filling of titanium t_{2g} levels and an ionic formulation is justified for Li_xTiO_2 (B) denoted by $Li_x^{x+}(TiO_2)^{x-}$. The average net charge of lithium in a hypothetical Li_1TiO_2 (B) is +0.98. Thus, in Fig. 12 the Fermi level is indicated for TiO_2 (B) and $Li_{0.5}TiO_2$ (B). In the next section we show what happens with these valence electrons after transferring them to the TiO_2 (B) host lattice.

By analogy with the lithium intercalation in anatase, COOP curves have been calculated for the Ti—Ti bonds in an idealized $Li_{0.5}TiO_2$ (B). In an idealized framework, every titanium is surrounded by three other titanium atoms with equal distances of 2.871 Å. The coordination is shown in Fig. 13. For simplicity the five different Ti—Ti bond types are labeled by [A], [B], [C], [D] and [E].

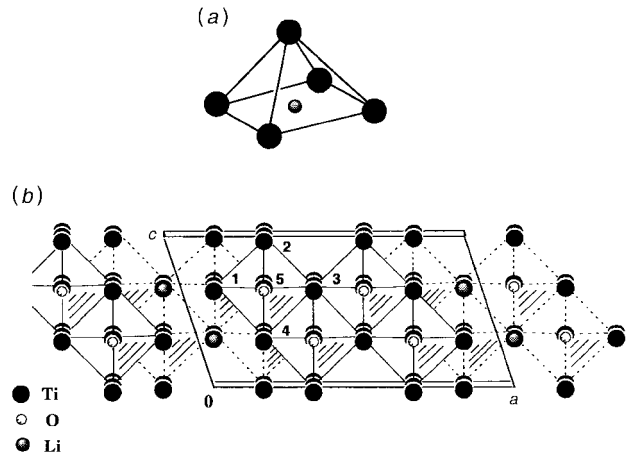

Fig. 11 (*a*) Square-pyramidal coordination polyhedron in LiO_5. (*b*) Penta-coordinated Li in the TiO_2 (B) lattice of $Li_{0.5}TiO_2$ (B).

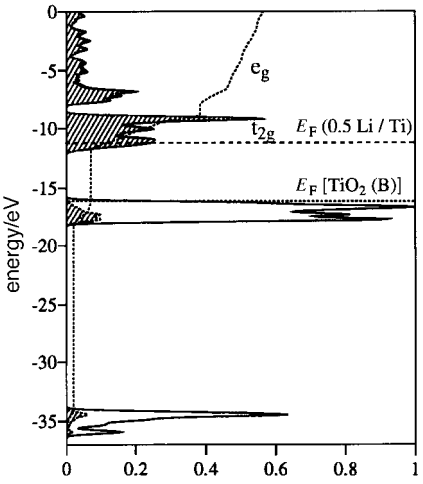

Fig. 12 DOS for an idealized TiO_2 (B) structure [d(Ti—O) = 2.03 Å]. Shaded regions correspond to the contribution of titanium and the dotted line running upwards indicates the integration of the projected titanium levels. The Fermi level is marked for TiO_2 (B) and for $Li_{0.5}TiO_2$ (B).

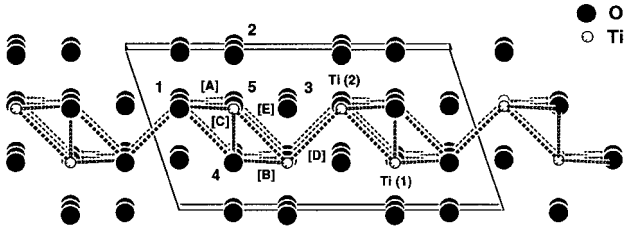

Fig. 13 Idealized $Li_{0.5}TiO_2$ (B) framework, with bonds [A]–[E] indicated

The COOP curves for the Ti—Ti bonds [A] and [B] in $Li_{0.5}TiO_2$ (B) are shown in Fig. 14 (the COOP curves for the other three Ti—Ti bonds are very similar). It is evident from inspection of Fig. 14 that bonding d levels are occupied when inserting up to 1 Li per Ti in the framework. This result indicates the formation of weak Ti—Ti bonds in Li_xTiO_2 (B) as we already derived for the intercalation in anatase. The resulting Ti—Ti zigzag chains formed along [100] and [010] direction are represented by double dashed lines in Fig. 13. Again, $\sigma(d^{Ti}–d^{Ti})$ interactions are responsible for the bonding character of the Ti—Ti bonds.

In contrast with the lithium intercalation in anatase, no distortion of the original framework is needed in TiO_2 (B) to achieve bonding interactions (*cf.* Fig. 7). This is a principal difference of the lithium insertion in both frameworks. Just beyond 1.25 Li per Ti strongly antibonding d levels would be filled in [A], [B] and [C]. In addition, the AOP for the different Ti—Ti bonds are shown as a function of lithium content in Fig. 15.

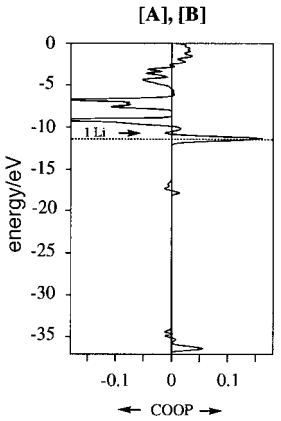

Fig. 14 COOP curves for the 'interlayer' Ti—Ti bonds [A] and [B] in an idealized $Li_{0.5}TiO_2$ (B) structure [d(Ti—O) = 2.03 Å]. The dotted horizontal line indicates the Fermi level for $Li_{0.5}TiO_2$ (B); the arrow indicates the energy level for 1 Li per Ti.

The general trend of the AOP is very similar to that of Li_xTiO_2 (A) (Table 1). In TiO_2 (B) itself, all Ti—Ti interactions show antibonding character, but with increasing lithium intercalation all Ti—Ti interactions change to more and more bonding character. Furthermore, Fig. 15 shows that the bonding character of [A], [B], [C] connecting Ti of different 'sheets' A and B in Fig. 2 is higher than that of [D] and [E]. In order to distinguish these two types of Ti—Ti bonds, we call the first 'interlayer' bonds and the second 'intralayer' bonds. Using this terminology, the 'interlayer' Ti—Ti bonds are stronger than the 'intralayer' bonds. As a consequence of these different bonding natures, there are two types of titanium atoms. The first one has two 'interlayer' and one 'intralayer' titanium neighbours, and the second one has one 'interlayer' and two 'intralayer' titanium neighbours. In Fig. 13 these two types are labelled as Ti(1) and Ti(2). By inserting lithium into the TiO_2 (B) lattice, also the total population of these different kind of titanium atoms splits as a function of increasing lithium content. This splitting of the total population is shown in Table 3.

A possible reason for this behaviour is that every Ti(1) forms two stronger and one weaker Ti—Ti bonds to its nearest titanium neighbours, whereas every Ti(2) forms only one stronger and two weaker Ti—Ti bonds. In a qualitative view the Ti(1) atoms will become more 'electronegative' than the Ti(2) atoms if d levels are filled up to 1e per Ti atom. These results suggest a small distortion of the ideal octahedral environment.

We do not present the COOP curves for the 10 different Ti—O bonds, because they show the same behaviour as those of anatase. In short, by following the arguments evaluated for

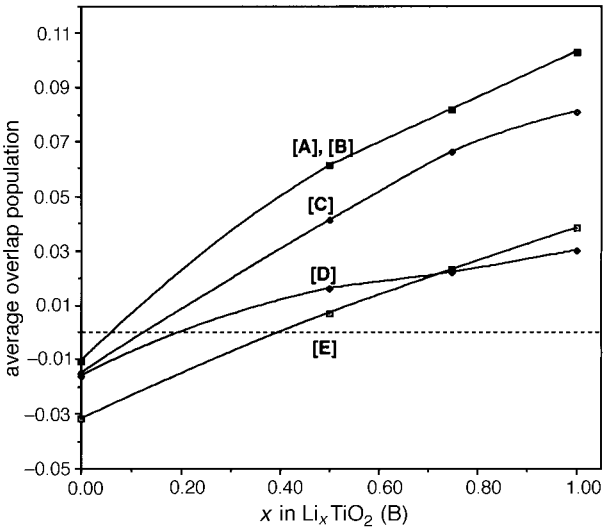

Fig. 15 Average overlap population of the Ti—Ti bonds as a function of lithium content x in an idealized Li_xTiO_2 (B) structure [d (Ti—O) = 2.03 Å]

Table 3 Total population of titanium (1) and (2) in Li_xTiO_2 (B) as a function of lithium content x

	TiO_2 (B)	$Li_{0.5}TiO_2$ (B)	$Li_{0.75}TiO_2$ (B)	$LiTiO_2$ (B)
Ti (1)	1.23	1.91	2.22	2.55
Ti (2)	1.27	1.73	1.88	2.04

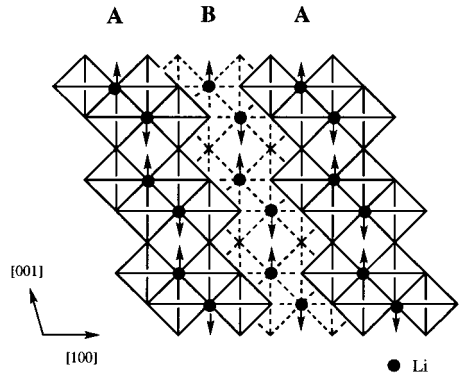

Fig. 16 Li—Li repulsion in $Li_{0.5}TiO_2$ (B); the arrows mark the directions of possible movement

anatase, the strength of the Ti—O bonds is hardly changed after lithium insertion.

In $Li_{0.5}TiO_2$ (B) one crystallographic site is completely occupied in the space group $C2/m$ by analogy with $Li_2FeV_3O_8$. In an idealized TiO_2 (B) framework (Fig. 2) the shortest Li—Li distance is 2.871 Å which is significantly longer than the shortest Li—Li distance in anatase (2.54 Å). Therefore it is not surprising that the AOP for this Li—Li distance indicates no bonding interaction. Compared to a hypothetical metallic Li chain with equal Li—Li distances of 2.871 Å, the total value of the AOP in Li_xTiO_2 (B) decreases to about 0.1. Thus, Coulombic nuclear–nuclear repulsion is likely to be the dominant force for the exact positions of the lithium atoms within the channels. Because of Coulombic repulsion the lithium ions will slightly move in opposite directions as shown by the arrows in Fig. 16.

In $Li_{0.5}TiO_2$ (B) the structure distorts so as to increase Li—Li distances. Such a displacement is also observed in $Li_2FeV_3O_8$ causing a small distortion of the ideal LiO_5 square pyramid.[48] If the lithium content increases up to a stoichiometry of $Li_{0.75}TiO_2$, the number of short Li—Li contacts will be doubled by forming one-dimensional Li—Li chains in the tunnels of the framework. A large movement of lithium in direction of the neighbouring oxygen in order to weaken the repulsive forces is not reasonable, because the Li—O distance is 2.03 Å. Typical Li—O distances in comparable compounds such as $Li_{0.5}TiO_2$ (anatase) and $Li_2FeV_3O_8$ are between 1.97 and 2.04 Å.[47,48] Thus, occupying all possible pentacoordinated sites in the channels leads to additional repulsive Li—Li contacts in a (hypothetical) $LiTiO_2$. Therefore, a further filling of the channels beyond a stoichiometry of $Li_{0.5}TiO_2$ becomes rather difficult. In practice, the lithium intercalation stops at a final amount of 0.8–0.85 Li per Ti.[29] Nevertheless, for smaller amounts of lithium up to about 0.5 Li per Ti, an easy migration of the inserted lithium ions is possible within the channels by 'hopping' from occupied to unoccupied pentacoordinated sites. This is an important property for the use of these materials as electrodes in solid-state batteries.

Conclusions

The main feature of the electronic properties of lithium intercalation in anatase and TiO_2 (B) is the formation of weak bonding Ti—Ti interaction. In both cases $\sigma(d^{Ti}–d^{Ti})$ interactions result in one-dimensional Ti—Ti zigzag chains. In anatase, only a small distortion of the framework is sufficient to change the expected antibonding Ti—Ti character of the original anatase framework to bonding character in $Li_{0.5}TiO_2$ (A). The small distortion causes an energetic shift of high lying bonding d levels below the Fermi level in $Li_{0.5}TiO_2$ (A). In anatase no Ti—O bond cleavage is necessary to balance the electronic and geometric stress during lithium incorporation. The strength of the Ti—O bonds mainly responsible for the stability of the framework is not necessarily affected by lithium insertion. The basic behaviour for TiO_2 (B) is very similar, but no distortion of the framework is needed to form Ti—Ti bonds.

Furthermore, in an idealized TiO_2 (B) structure the computational results indicate two types of titanium atoms with different average net charges or 'electronegativities'. As a consequence, a small distortion of this framework is likely to be reasonable.

Table 4 Extended Hückel parameters[49–52]

	orbital	H_{ii}/eV	ζ_1
Li	2s	−5.342	0.645
	2p	−3.499	0.524
O	2s	−34.024	2.192
	2p	−16.768	2.018
Ti	4s	−6.039	1.195
	4p	−3.863	0.998
	3d[a]	−11.043	4.2180

[a] $\zeta_2 = 1.6640$, $c_1 = 0.4690$, $c_2 = 0.686$.

Appendix

The program YAeHMOP ('Yet another extended Hückel Molecular Orbital Package'),[49] an extended Hückel implementation of the tight binding method, was used in all calculations. Table 4 lists the parameters for the elements which are used in this work.[50–52] A 64 k-point set was used for anatase and $Li_{0.5}TiO_2$ and 27 k-points for TiO_2 (B) and $Li_{0.5}TiO_2$ (B). These mesh points in the irreducible wedge of the Brillouin zone were generated using the geometrical method of Ramirez and Boehm.[53]

This work was supported by a Grant-in-Aid for Scientific Research from the Ministry of Education, Science and Culture of Japan and by the Japan Society for the Promotion of Science (JSPS-RFTF96P00206). G.N. is grateful to the JSPS for financial support, which made his stay at the Institute for Fundamental Chemistry possible.

References

1 M. S. Whittingham, *Prog. Solid State Chem.*, 1978, **12**, 1.
2 M. S. Whittingham, *Science*, 1976, **192**, 1126.
3 M. S. Whittingham, *J. Electrochem. Soc.*, 1976, **123**, 315.
4 D. W. Murphy and F. A. Trumbore, *J. Cryst. Growth*, 1977, **39**, 185.
5 G. L. Holleck and J. R. Driscoll, *Electrochim. Acta*, 1977, **22**, 647.
6 J. O. Besenhard and R. Schöllhorn, *J. Power Sources*, 1976, **1**, 267.
7 B. C. Steele, in *Superionic Conductors*, ed. G. D. Mahan and W. L. Roth, Plenum Press, New York, 1976, p. 47.
8 P. Palvadeau, L. Coic, J. Rouxel and J. Portier, *Mater. Res. Bull.*, 1978, **13**, 221.
9 A. H. Thomson, *J. Electrochem. Soc.*, 1979, **126**, 608.
10 M. S. Whittingham, *J. Electrochem. Soc.*, 1976, **123**, 315.
11 R. H. Friend and A. D. Yoffee, *Adv. Phys.*, 1987, **36**, 1.
12 C. Julien, I. Samaras, O. Gorochov and A. M. Ghorayeb, *Phys. Rev. B*, 1992, **45**, 13390.
13 F. Mendizabal, R. Contreras and A. Aizman, *Int. J. Quantum Chem.*, 1995, **56**, 819.
14 D. W. Murphy and P. A. Christian, *Science*, 1979, **205**, 651.
15 D. W. Murphy, P. A. Christian, F. J. DiSalvo, J. N. Carides and J. V. Waszczak, *J. Electrochem. Soc.*, 1981, **128**, 2053.
16 B. Zachau-Christiansen, K. West and T. Jacobsen, *Mater. Res. Bull.*, 1985, **20**, 485.
17 R. J. Wiseman and P. G. Dickens, *J. Solid State Chem.*, 1976, **17**, 91.
18 D. E. Cox, R. J. Cava, D. B. McWhan and D. W. Murphy, *J. Phys. Chem. Solids*, 1982, **43**, 657.
19 R. J. Cava, A. Santoro, D. W. Murphy, S. Zahurak and R. S. Roth, *J. Solid State Chem.*, 1982, 42, 251.
20 B. O'Regan, J. Moser, M. Anderson and M. Grätzel, *J. Phys. Chem.*, 1990, **94**, 8720.
21 S. Huang, L. Kavan, A. Kay and M. Grätzel, *Act. Pass. Elec. Comp.*, 1995, **18**, 23.

22 S. Huang, L. Kavan, I. Exnar and M. Grätzel, *J. Electrochem. Soc*., 1995, **142**, L142.
23 F. Bonino, M. Lazzari and L. P. Bicelli, *Proc. Electrochem. Soc*., 1981, **81**, 255.
24 M. Voinov, *Proc. Electrochem. Soc*., 1981, **81**, 352.
25 S. Yoshizawa, Z. Takehara, T. Nishimura and I. Makino, in *Ext. Abstr., 32nd ISE Meeting*, Dubrovnik, 1981.
26 F. Bonino, L. Busani, M. Manstretta, B. Rivolta and B. Scrosati, *J. Power Sources*, 1978, **6**, 261.
27 D. W. Murphy, F. J. Di Salvo, J. N. Carides and J. V. Waszczak, *Mater. Res. Bull*., 1978, **13**, 1395.
28 T. Ohzuku, Z. Takehara and S. Yoshizawa, *Electrochim. Acta*, 1979, **24**, 219.
29 B. Zachau-Christiansen, K. West, T. Jacobsen and S. Atlung, *Solid State Ionics*, 1988, **28**, 1176.
30 M. S. Whittingham and M. B. Dines, *J. Electrochem. Soc*., 1977, **124**, 1387.
31 D. W. Murphy, M. Greeblatt, S. M. Zahurak, R. C. Cava, J. V. Waszczak, G. W. Hull, Jr. and R. S. Hutton, *Rev. Chim. Miner*., 1982, **19**, 441.
32 D. Bi, J. Wang, Y. Sun and Z. Liao, *Proc. Electrochem. Soc*., 1980, **80**, 245.
33 T. Ohzuku, T. Kodama and T. Hirai, *J. Power Sources*, 1985, **14**, 261.
34 D. Bi, J. Wang and Y. Sun, in *Power Sources*, ed. J. Thompson, Academic Press, New York, 1984.
35 T. Ohzuku and T. Hirai, *Electrochim. Acta*, 1982, **27**, 1263.
36 R. Marchand, L. Brohan and M. Tournoux, *Mater. Res. Bull*., 1980, **15**, 1129.
37 L. Brohan and R. Marchand, *Solid State Ionics*, 1983, **9**/**10**, 419.
38 L. Pauling and J. H. Sturdivant, *Z. Kristallogr. A, Kristallgeom., Kristallphys., Kristallchem*., 1928, **68**, 239.
39 W. H. Baur, *Acta Crystallogr*., 1961, **14**, 214.
40 D. T. Cromer and K. Herrington, *J. Am. Chem. Soc*., 1955, **77**, 4708.
41 T. M. Sabine and C. H. Howard, *Acta Crystallogr., Sect. B,* 1982, **38**, 701.
42 W. H. Baur and A. A. Khan, *Acta Crystallogr., Sect. B,* 1971, **27**, 2133.
43 R. Restori, D. Schwarzenbach and J. R. Schneider, *Acta Crystallogr*., 1987, **43**, 251.
44 A. Stashans, S. Lunell, R. Bergstroem, A. Hagfeldt and S.-E. Lindquist, *Phys. Rev. B*, 1996, **53**, 159.
45 T. Hughbanks and R. Hoffmann, *J. Am. Chem. Soc*., 1983, **105**, 3528.
46 R. Hoffmann, *J. Chem. Phys*., 1963, **39**, 1397.
47 R. C. Cava, D. W. Murphy, S. Zahurak, A. Santoro and R. S. Roth, *J. Solid State Chem*., 1984, **53**, 64.
48 R. J. Cava, A. Santoro, D. W. Murphy, S. M. Zahurak and R. S. Roth, *J. Solid State Chem*., 1983, **48,** 309.
49 G. A. Landrum, YAeHMOP (Yet Another extended Hückel Molecular Orbital Package), Version 1.2, Cornell University, Ithaca, NY, 1996.
50 E. Muller, Tables of Parameters for extended Hückel Calculations (Edgar.Muller@icma.unil.ch), available in YAeHMOP 1.2.[49]
51 P. Pyykkö and L. L. Lohr, Jr., *Inorg. Chem*., 1981, **20**, 1950.
52 N. J. Fitzpatrick and G. H. Murphy, *Inorg. Chim. Acta*, 1986, **111**, 139.
53 R. Ramirez and M. C. Boehm, *Int. J. Quantum Chem*., 1988, **34**, 571.

Paper 7/03935B; *Received* 5*th June*, 1997